

Ferric iron in magmatic clinopyroxene, Part I: re-evaluating stoichiometric estimates of iron valence with implications for clinopyroxene componentry

David A. Neave*, Alexander G. Stewart, Margaret E. Hartley, Catherine McCammon

*david.neave@manchester.ac.uk

This is a non-peer reviewed preprint of an article submitted for publication in Contributions to Mineralogy and Petrology and uploaded to EarthArXiv in June 2023.

Ferric iron in magmatic clinopyroxene, Part I: re-evaluating stoichiometric estimates of iron valence with implications for clinopyroxene componentry

David A. Neave^{1*}, Alexander G. Stewart¹, Margaret E. Hartley¹,
Catherine McCammon²

^{1*}Department of Earth and Environmental Sciences, The University of
Manchester, Manchester, M13 9PL, United Kingdom.

²Bayerisches Geoinstitut, Universität Bayreuth, 95440 Bayreuth,
Germany.

*Corresponding author(s). E-mail(s): david.neave@manchester.ac.uk;

Abstract

Clinopyroxene is a major rock forming mineral capable of incorporating a wide range of metal cations. As a consequence, clinopyroxene preserves valuable archives of magmatic processes and understanding clinopyroxene is essential for understanding Earth's broader chemical evolution. However, knowledge about the relative abundances of ferrous and ferric iron in magmatic clinopyroxenes remains poor because it is not currently possible to routinely measure the valence of iron in clinopyroxene crystals without either separating single crystals for bulk analysis or securing access to Mössbauer spectroscopy or a synchrotron radiation source to perform *in-situ* microanalysis. This is despite many magmatic clinopyroxene crystals seemingly containing appreciable quantities of ferric iron, highlighting the potential for developing widely applicable clinopyroxene-based oxybarometers. Here we integrate optimised electron probe microanalysis and Mössbauer spectroscopy on endmember and single-crystal clinopyroxenes to re-evaluate previously discredited approaches for estimating clinopyroxene ferric iron contents by stoichiometry. By ensuring that all major and minor elements in clinopyroxene crystals are measured with sufficient precision, we show that it is possible to readily obtain stoichiometric estimates of clinopyroxene ferric to total iron contents with similar precisions to those derived from Mössbauer spectroscopy ($1\sigma \sim 3.5\%$ absolute). Being able to robustly determine clinopyroxene ferric iron contexts enables us to propose a new scheme for assigning

clinopyroxene components that explicitly accounts for ferric iron, which is primarily hosted within esseneite component ($\text{CaFe}^{3+}\text{AlSiO}_6$) in clinopyroxenes dominated by quadrialteral components and aegirine component ($\text{NaFe}^{3+}\text{Si}_2\text{O}_6$) in alkali clinopyroxenes. Our new scheme provides a framework for documenting the full spectrum of clinopyroxene compositions in studies on both natural and experimental systems.

Keywords: clinopyroxene, ferric iron, stoichiometry, oxygen fugacity

1 Introduction

Clinopyroxene is a major constituent of diverse upper mantle and crustal rocks across all tectonic settings. This geologically significant mineral has the general formula $\text{M}_2(\text{R}^{2+})\text{M}_1(\text{R}^{2+})\text{T}_2(2\text{R}^{4+})\text{O}_6$, where R is a metal cation, M2 is a distorted octahedral site, M1 is a regular octahedral site and T is a tetrahedral site typically occupied by Si forming the Si_2O_6 chains that define the pyroxene structure (Mori-moto et al, 1988). This variety of sites enables clinopyroxene to incorporate most of the major metal cations that occur in terrestrial magmas, making it a particularly valuable tool for reconstructing the thermochemical evolution of magmatic systems in space and time (e.g., Putirka et al, 1996; Wood and Blundy, 1997; Mollo et al, 2010; Petrone et al, 2016; Ubide and Kamber, 2018). However, the compositional complexity resulting from this mineralogical plasticity also makes it challenging to model clinopyroxene-liquid equilibria (e.g., Sack and Ghiorso, 1994a; Green et al, 2007) and unambiguously disentangle the processes that crystal compositions record in both natural and experimental systems (e.g., Mollo et al, 2013; Neave et al, 2019; Ubide et al, 2019). Although understanding the chemistry of clinopyroxene is vital for understanding the chemical evolution of planetary interiors, much about this abundant and geologically useful mineral remains poorly understood. For example, knowledge about the relative abundances of ferrous and ferric iron (Fe^{2+} and Fe^{3+} , respectively) in magmatic clinopyroxenes, as well as their respective partitioning behaviours, is especially sparse. This is despite the ability of clinopyroxene to incorporate both Fe^{2+} and Fe^{3+} and potentially record information about magmatic oxygen fugacity (f_{O_2}) by serving as an oxybarometer. Developing a clinopyroxene-based oxybarometer could generate new insights into important and redox-dependent processes including magmatic evolution, ore mineralisation and volcanic degassing (Frost, 1991).

Oceanic basalts (mafic igneous rocks erupted in mid-ocean ridge and ocean-island settings), which dominate Earth's magma budget, frequently contain significant quantities of augitic clinopyroxene. Augite has the general formula $\text{Ca}(\text{Mg},\text{Fe}^{2+})\text{Si}_2\text{O}_6$ and is the mineral name given to the solid solution between Mg-rich diopside (Di; $\text{CaMgSi}_2\text{O}_6$) and Fe^{2+} -rich hedenbergite (Hd; $\text{CaFe}^{2+}\text{Si}_2\text{O}_6$; Deer et al, 2013). Augite, diopside and hedenbergite have standard site occupancies, with Ca^{2+} on their M2 sites, Mg^{2+} and Fe^{2+} (and minor Mn^{2+}) on their M1 sites and tetravalent Si^{4+} on their T sites. However, pure augite is rare in nature, with most natural crystals incorporating small amounts of Ca-poor enstatite (En; $\text{Mg}_2\text{Si}_2\text{O}_6$) and ferrosilite (Fs; $\text{Fe}_2^{2+}\text{Si}_2\text{O}_6$)

components alongside various additional components. One of the most prevalent substitutions responsible for the incorporation of additional components involves the coupled substitution of R^{2+} on the M1 site and R^{4+} on one T site with R^{3+} on both. For example, $(Mg,Fe)^{2+}$ and Si^{4+} are commonly replaced with Al^{3+} to create calcium Tschermak's component (CaTs; $CaAlAlSiO_6$). Indeed, that the Al_2O_3 content of clinopyroxene crystals from oceanic basalts ranges from ~ 2 wt.% in tholeiitic mid-ocean-ridge and Icelandic basalts (e.g., Bryan et al, 1981; Jakobsson et al, 1978) to >10 wt.% in alkaline basanites and ankaramites from the Canary Islands and Hawaii (e.g., Klügel et al, 2005; Hammer et al, 2016) attests to the importance of Al-rich components in natural clinopyroxene crystals. The componentry scheme of Putirka et al (2003) also incorporates Cr^{3+} , which occurs at levels up to 2 wt.% Cr_2O_3 in some primitive augite crystals (MacLennan et al, 2003) via a similar substitution to form chromium calcium Tschermak's component (CrCaTs; $CaCrCrSiO_6$).

The substitution of R^{2+} on M2 and M1 sites with R^{1+} on the M2 site and R^{3+} on the M1 site is of particular geological utility because the formation of the Na^{1+} - and Al^{3+} -bearing jadeite component (Jd; $NaAlSi_2O_6$) depends strongly on pressure and can therefore be exploited as a barometer (Blundy et al, 1995; Putirka et al, 1996). Specifically, the large partial molar volume change associated with Jd formation means that clinopyroxene formed at high pressure contain more Jd and therefore more Na than that formed from similar melts at low pressure, a phenomenon that has been exploited in the calibration of diverse clinopyroxene-based geobarometers (e.g., Putirka et al, 1996; Putirka, 2008; Neave and Putirka, 2017; Wang et al, 2021). Another important and analogous substitution concerns the formation of the Na^{1+} - and Fe^{3+} -bearing aegirine component (Ae; $NaFe^{3+}Si_2O_6$). Clinopyroxene crystals dominated by Ae, simply referred to as aegirine, are commonly found in highly evolved alkaline rocks like those from the Ilímaussaq intrusion in Greenland (e.g., Larsen, 1976), though Ae-rich augite (aegirine-augite) also occurs in less extreme alkaline differentiates like those found on Pantelleria, Italy (e.g., White et al, 2005). However, the importance of the Ae component in clinopyroxene from oceanic basalts remains unclear. This is partly because of their low Na contents and partly because of uncertainties about the abundance of Fe^{3+} in clinopyroxene crystals from oceanic basalts as well as the mechanisms by which it is incorporated.

Augite contains significant amounts of Fe, which is typically reported assuming that all Fe is Fe^{2+} (i.e., FeO_T) because it is impossible to determine Fe valence from routine $FeK\alpha$ emission spectroscopy by electron probe microanalysis (EPMA). Measuring $FeL\alpha$ and $FeL\beta$ emission lines can provide information about Fe valence but remains to be demonstrated conclusively for clinopyroxene (Smith and O'Nions, 1971; Höfer et al, 1994; Höfer and Brey, 2007). Nonetheless, the few direct determinations of Fe valence in magmatic clinopyroxene crystals available from Mössbauer spectroscopy suggest that ratios of Fe^{3+} to total Fe (i.e., $Fe^{3+}/\Sigma Fe$) are well above zero in many cases and can reach up to 0.6 in crystals from mafic alkaline rocks erupted in the Canary Islands and elsewhere (McGuire et al, 1989; Weis et al, 2015), in line with legacy wet chemical datasets (e.g., Deer et al, 2013). This variability in clinopyroxene $Fe^{3+}/\Sigma Fe$ is perhaps unsurprising given that glass $Fe^{3+}/\Sigma Fe$ contents spanning the range ~ 0.14 – 0.35 have now been documented in Fe X-ray absorption near edge

structure (Fe-XANES) spectroscopy studies of oceanic basalts (Shorttle et al, 2015; Moussallam et al, 2016; Brounce et al, 2017; Zhang et al, 2018; Moussallam et al, 2019). Overall, these observations imply that Fe^{3+} is a cryptic but significant constituent of clinopyroxenes from oceanic basalts. The relatively low Na content of most magmatic augite crystals (usually <1 wt.% Na_2O ; Wieser et al, 2023) precludes the significant incorporation of Fe^{3+} as an Ae component because there is insufficient Na^{1+} to balance all of the Fe^{3+} present. Comparisons with mantle clinopyroxenes and the apparent insensitivity of Jd formation to f_{O_2} suggest that Fe^{3+} could be incorporated as esseneite component (Es; $\text{CaFe}^{3+}\text{AlSiO}_6$) via a Tschermak-type substitution (Luth and Canil, 1993; Neave et al, 2019). However, the systematic determinations of $\text{Fe}^{3+}/\Sigma\text{Fe}$ in magmatic clinopyroxenes needed to substantiate this suggestion remain elusive.

Mössbauer spectroscopy provides an accurate and precise way of determining clinopyroxene $\text{Fe}^{3+}/\Sigma\text{Fe}$ (e.g., McGuire et al, 1989; Canil and O'Neill, 1996; Sobolev et al, 1999). However, few labs have the necessary equipment and capacity to process large numbers of samples. Moreover, analytical spot sizes typically exceed 100 μm (though with important exceptions; McCammon, 1994), making the technique of limited use for studying magmatic crystals. Although crystal anisotropy makes it challenging to use Fe-XANES spectroscopy to determine clinopyroxene $\text{Fe}^{3+}/\Sigma\text{Fe}$ (Dyar et al, 2002; Steven et al, 2022), the recent use of oriented and Mössbauer-calibrated standards suggests that clinopyroxene Fe-XANES is a tractable prospect (Rudra et al, 2021; Rudra and Hirschmann, 2022), though the approach has yet to be applied to natural sample suites and ultimately depends on competitive access to synchrotron radiation sources. Applying stoichiometric criteria to EPMA data provides an alternative way to estimate $\text{Fe}^{3+}/\Sigma\text{Fe}$. One approach proposed by Papike (1974) and further popularised by Lindsley (1983) balances Na^{1+} on the M2 site and Al^{3+} on T sites with Al^{3+} , Cr^{3+} , Fe^{3+} and Ti^{4+} on the M1 site ($\text{Na} + \text{Al}^{\text{IV}} = \text{Al}^{\text{VI}} + \text{Cr} + \text{Fe}^{3+} + 2\text{Ti}^{4+}$). A more general approach proposed Droop (1987) estimates the amount of Fe^{3+} from the excess cations remaining after calculating clinopyroxene formulae on a six-oxygen basis. Specifically, Droop (1987) suggests that the amount of Fe^{3+} per X oxygens (where $X = 6$ for clinopyroxene), F , is given by:

$$F = 2X(1 - T/S), \quad (1)$$

where T is the ideal number of cations (where $T = 4$ for clinopyroxene), and S is the observed cation total per X oxygens when all Fe is assumed to be Fe^{2+} . Unfortunately, considerable doubt surrounds using stoichiometry to determine clinopyroxene $\text{Fe}^{3+}/\Sigma\text{Fe}$, with McGuire et al (1989) suggesting that it may be associated with absolute uncertainties of 25%, essentially rendering the approach useless for geology, a conclusion reinforced by the sensitivity assessment performed by Canil and O'Neill (1996). However, recent re-evaluations of uncertainties in clinopyroxene analyses by EPMA suggest that poorly optimised conditions may have resulted in poor precision in many legacy datasets, especially concerning the analysis of minor elements like Na, Cr and Mn that are relevant for thermobarometry (Wieser et al, 2023). Poor precision may have also compromised the ability to estimate $\text{Fe}^{3+}/\Sigma\text{Fe}$ by stoichiometry, which is ultimately dependent the accurate and precise calculation of cation sums. We

aim to critically re-evaluate the utility of stoichiometry as an accessible approach for determining clinopyroxene $\text{Fe}^{3+}/\Sigma\text{Fe}$ in light of advances in EPMA techniques.

Clinopyroxene compositions reported as element oxides are often recast into end-member components that notionally reflect the incorporation of diverse clinopyroxene components (real and fictive) via multiple solid solutions (e.g., Di–Hd and DiHd–Jd) into a single solid phase. As well as providing a convenient way to summarise clinopyroxene compositions, these components often serve endmembers in both empirical and thermodynamic models used to address geological problems (Lindsley, 1983; Sack and Ghiorso, 1994a; Putirka et al, 1996; Holland and Powell, 1998; Jennings and Holland, 2015). This is because mineral-melt and mineral-mineral reactions may often only take place between a subset of components. For example, Fe^{2+} –Mg exchange between clinopyroxene and melt will only directly affect Mg and Fe^{2+} bearing quadrilateral components (Di, Hd, En and Fs directly); effects on non-quadrilateral components (like Jd or CaTs) will be indirect. However, most schemes currently available for assigning clinopyroxene components either make now discredited assumptions about the components present or fail to account for the full range of elements present in natural crystals, limiting their usefulness. In particular, the widely used scheme described by Putirka et al (1996) and modified Putirka et al (2003) does not account for the presence of Fe^{3+} , while the scheme described by Lindsley (1983) assumes that all Fe^{3+} is balanced by Na in Ae and does not consider Ti despite its prevalence in many augite crystals Leung (1974). We aim to provide a new scheme for assigning clinopyroxene components that provides a more holistic reflection of clinopyroxene compositions that will support future work.

Here we present high-precision EPMA analyses of endmember and single-crystal clinopyroxenes on which we have also performed Mössbauer spectroscopy in order to critically re-evaluate the utility of determining clinopyroxene $\text{Fe}^{3+}/\Sigma\text{Fe}$ by stoichiometry. Having established that stoichiometry can indeed provide robust estimates of clinopyroxene $\text{Fe}^{3+}/\Sigma\text{Fe}$ we use our analyses to propose a revised scheme for assigning clinopyroxene components that explicitly accounts for all cations present including Fe^{3+} . This scheme will allow enable more robust comparisons of clinopyroxene compositions across diverse natural and experimental samples including the ocean island basalts (OIBs) discussed in Part II that will further unlock clinopyroxene’s potential as an archive of magmatic processes and magmatic f_{O_2} in particular.

2 Samples

We collated seven endmember and single-crystal clinopyroxenes from mineral collections hosted by Manchester Museum (MM) and the Department of Earth and Environment Sciences (DEES) at The University of Manchester (Table 1). In summary, we collated two aegirine crystals from evolved alkaline igneous rocks, two augite crystals from mafic alkaline rocks, one diopside crystal, one block of intergrown hedenbergite crystals from a skarn and one sample of intergrown clinopyroxene crystals of unclear affinity (labelled as diopside but described below as other). Single crystals were cut into at least four pieces, with three pieces being roughly oriented and mounted in

epoxy for microanalysis (including Fe-XANES spectroscopy to be described in a subsequent contribution) and one piece being powdered under isopropanol in an agate mortar and sandwiched between cellophane in ~ 0.5 mm diameter holes in 0.5 mm-thick wafers of Pb foil for Mössbauer spectroscopy. Multiple wafers were prepared for samples containing low total Fe contents. One important exception concerns the piece of augite 2 used for Mössbauer spectroscopy, which was obtained by mechanically separating part of a crystal identified as being free from Fe-Ti oxide inclusions (see below). Intergrown samples of hedenbergite and the other clinopyroxene were also mounted in epoxy for microanalysis after mechanically removing chips to powder for Mössbauer spectroscopy.

3 Methods

3.1 Microscopy

Epoxy mounts of endmember and single-crystal clinopyroxenes were investigated with a FEI Quanta 650F scanning electron microscope (SEM) in the Department of Earth and Environmental Sciences at The University of Manchester to characterise compositional variability within and between samples. Backscattered electron (BSE) images were used to identify targets for microanalysis that avoided inclusions and chemical heterogeneities as well as to screen samples for their suitability for bulk analysis by Mössbauer spectroscopy. Clinopyroxene compositions were also semi-quantitatively determined by energy dispersive X-ray spectroscopy (EDS) using an Bruker Quantax system to ensure that the correct elements were selected for quantitative analysis by EPMA. Measuring all minor elements present in EDS spectra is vital for properly quantifying clinopyroxene compositions (Wieser et al, 2023).

3.2 Electron probe microanalysis

Quantitative analyses were performed by EPMA using a JEOL JXA8530F instrument in the School of Earth Sciences at the University of Bristol operated with Probe for EPMA (<https://www.probesoftware.com/>). The following primary standards were used for calibration: Si, albite; Ti, TiO₂; Al, sanidine; Cr, Cr₂O₃; Fe, hematite; Mn, Mn metal; Mg, St. John’s Island olivine; Ca, wollastonite; Na, albite; K, sanidine; P, Durango apatite; and Ni, Ni metal.

Particular care was taken over the analysis of clinopyroxene to enable us to re-evaluate whether clinopyroxene $\text{Fe}^{3+}/\Sigma\text{Fe}$ could be determined by stoichiometry. We used an accelerating voltage of 15 kV and a spot size of 1 μm . The following elements were analysed with a current of 10 nA (on-peak counting times in seconds are shown in parentheses; background counting times were half on-peak counting times on each side of the peak): Si(20), Ti(20), Al(20), Fe(40), Mg(40), Ca(20) and K(40); and the following elements were analysed with a current of 40 nA: Cr(60), Mn(30), Na(60), P(60) and Ni(30). We used this approach to maximise the precision of minor element analyses. This is because the quality of minor element analyses is known to affect the performance of thermobarometric calculations (Wieser et al, 2023), and we hence suspect that it may also affect the precision of clinopyroxene $\text{Fe}^{3+}/\Sigma\text{Fe}$ determinations

by stoichiometry. We suggest that a realistic aim when measuring clinopyroxene by EPMA is to analyse each element at a sufficient current and for a sufficiently long time to return 1σ precisions from counting statistics on the order of 2% or better for major elements and 5% or better for minor elements. Importantly, monitoring the time-dependent intensity of Na counts has demonstrated that Na remains immobile when analysing augitic clinopyroxene crystals with a focused beam at 40 nA or even 100 nA (Wieser et al, 2023). Nonetheless, we recommend verifying that unknowns are stable under the beam conditions in question prior to analysis.

Accuracy was monitored by analysing the following secondary standards: an in-house diopside, an in-house Cr-diopside and kk1 kaersutite (Reay et al, 1989). Major element (e.g., SiO_2 and MgO) concentrations were typically within 2% of preferred values (based on published values or longitudinal data for in-house standards), while minor element (e.g., Cr_2O_3 and Na_2O in Cr-diopside) concentrations were typically within 6% of preferred values. However, validating the accuracy of minor element analyses with international clinopyroxene standards is challenging because of lingering uncertainties about standard homogeneity (Fournelle and Scott, 2017). While no standard is perfect, we suggest that the Cr augite (NMNH 164905) described by Jarosewich et al (1987), which was unfortunately unavailable for our EPMA sessions, is probably the best widely available material for validating EPMA accuracy for determining clinopyroxene $\text{Fe}^{3+}/\Sigma\text{Fe}$. Counting statistics from analyses of unknown clinopyroxene crystals indicate that major (SiO_2 , Al_2O_3 , FeO_T , MgO and CaO) and minor (TiO_2 , Cr_2O_3 and Na_2O) elements were measured with 1σ precisions better than 1% and 5%, respectively; only MnO was measured with a worse 1σ precision of $\sim 8\%$. Full details of secondary standard analyses and analytical precision are provided in the Supplementary Material alongside all EPMA data.

3.3 Mössbauer spectroscopy

Mössbauer spectroscopy was performed on powdered endmember and single-crystal clinopyroxenes sandwiched between cellophane in holes in 0.5 mm-thick wafers of Pb. Multiple wafers were prepared for samples with low FeO_T contents (<5 wt.%) to ensure that effective sample thicknesses were sufficient for high quality analyses (McCammon, 2021). Spectra were collected using a constant acceleration Mössbauer spectrometer with a nominal 450 MBq ^{57}Co high specific activity source in a 12 μm -thick Rh matrix in the Bayerisches Geoinstitut at the Universität Bayreuth. Velocity scales were calibrated against a 25 μm -thick α -Fe foil using positions from standard reference material 1541 of the (former) National Bureau of Standards. Outer line widths of 0.36 mm/s were obtained for α -Fe at room temperature. Spectra were fitted with the MossA programme described by Prescher et al (2012) using two or three doublets assigned variably to Fe^{2+} and Fe^{3+} depending on the complexity of the spectra produced; the fit for aegirine 2 was improved by the inclusion of an additional singlet assigned to Fe^{3+} . The quality of Lorentzian fits to Mössbauer spectra indicates that 1σ analytical uncertainties in $\text{Fe}^{3+}/\Sigma\text{Fe}$ determinations are 0.02–0.03 absolute for all samples except the other clinopyroxene, which was subject to a slightly larger absolute uncertainty of 0.05 because of its low FeO_T content and compositional heterogeneity (see below). MossA fits are provided in the Supplementary Figures 1 and 2.

4 Results

4.1 Clinopyroxene textures

Characteristic textures of endmember and single-crystal clinopyroxenes observed via BSE image are shown in Figure 1. Neither aegirine 1 nor aegirine 2 show clear evidence for internal compositional zoning, though the former hosts fractures with low volumes of low- and high-BSE-intensity phases and the latter contains diffuse bands of small crystals with high BSE intensities (Figures 1A and B, respectively). While too small to measure by EPMA, EDS analyses suggest that the high-BSE-intensity phases are Fe-Ti oxides. While such oxides could compromise bulk $\text{Fe}^{3+}/\Sigma\text{Fe}$ determinations, they make up much less than 1 vol.% of the crystals and would therefore exert little leverage over the resulting Mössbauer spectra, especially given the high FeO_T of the aegirine crystals in question. Most pieces of augite 1 show no evidence for compositional zoning (Figure 1C), though minor core-rim zoning can be seen on some places (Supplementary Figure 3). Occasional Fe-Ti oxide inclusions are sufficiently infrequent to have minimal effect on Mössbauer spectra. Despite showing no evidence for compositional zoning, augite 2 contains abundant and large Fe-Ti oxide inclusions (Figure 1D). However, material for Mössbauer spectroscopy was mechanically sampled from an inclusion-poor portion of the crystal, reducing the risk of contamination. The diopside crystal is homogenous and inclusion-free (Figure 1E), while the other clinopyroxene is inclusion free but clearly compositionally zoned in complex ways that could not be mitigated during sampling for Mössbauer spectroscopy (Figure 1F). The hedenbergite sample contains intergrown and compositionally homogeneous crystals (Supplementary Figure 4).

4.2 Major element chemistry

The major element chemistry of endmember and single-crystal clinopyroxenes is summarised in Figure 2 and Table 1. The Q-J diagram in Figure 2A demonstrates that all of the endmember and single-crystal clinopyroxenes we describe with the exception of the two Na-rich aegirine crystals are dominated by quadrilateral components (Morimoto et al, 1988). With a similar exception of the two aegirine crystals, all of the other endmember and single-crystal clinopyroxenes fall along the Di-Hd tie line on the pyroxene quadrilateral in which the Fe component (ΣFe^*) is equal to the sum of Fe^{2+} , Fe^{3+} and Mn (Figure 2B; Morimoto et al, 1988). The diopside and other clinopyroxene fall close to the Di apex, the hedenberite falls close to the Hd apex, and, as expected, the aegirine crystals fall close to the Fs apex by virtue of their high Fe content but low Ca content. The two augite crystals fall between the Di and Hd apices and contain very little En and Fs component by this reckoning.

Endmember and single-crystal clinopyroxene Na_2O contents are summarised in Figure 3A. Excluding the aegirine crystals that contain $\sim 12\text{--}13$ wt.% Na_2O , our clinopyroxene crystals contain 0.1–0.5 wt.% Na_2O , with the augite crystals being relatively enriched in Na in comparison with the diopside and hedenbergite. Almost all endmember and single-crystal clinopyroxenes contain very low concentrations of Cr_2O_3 with only the diopside and augite 1 (and one piece of augite 3) containing appreciable

but variable Cr_2O_3 contents indicative of internal zoning (Figure 3B). Variations in Ti and Al contents are shown in Figure 3C. Only the augite crystals contain meaningful concentrations of both Al and Ti that fall along lines of constant Ti:Al. Both aegirine crystals contain significant but different and variable amounts of Ti.

4.3 Iron concentration and valence systematics

The FeO_T content of endmember and single-crystal clinopyroxenes is summarised in Figure 4A, and ranges from $\sim 1\text{--}3$ wt.% in the diopside and other clinopyroxene through ~ 7 wt.% in the augite crystals to $\sim 26\text{--}29$ wt.% in the aegirine crystals and hedenbergite. Although analytical uncertainty is the main control over FeO_T variability in some clinopyroxene crystals (augite 2, aegirine 2 and hedenbergite), other clinopyroxene crystals show variability consistent with the intra-mineral compositional zoning (augite 1, aegirine 1 and the other clinopyroxene), which is visible in BSE images of some crystals (e.g., Fig 1F).

Endmember and single crystal clinopyroxene $\text{Fe}^{3+}/\Sigma\text{Fe}$ contents determined by Mössbauer spectroscopy are summarised as a function of FeO_T in Figure 4B and are provided in Table 1. Although multiple pieces of these clinopyroxene crystals ($n = 2\text{--}5$) were analysed multiple times by EPMA to produce the piece-wise mean compositions plotted in Figure 4B and sample-wise mean concentrations collated in Table 2 ($n = 3\text{--}10$ per piece and $n = 12\text{--}36$), only one Mössbauer analysis was performed per sample. Uncertainties in $\text{Fe}^{3+}/\Sigma\text{Fe}$ do not vary strongly with FeO_T or $\text{Fe}^{3+}/\Sigma\text{Fe}$. As anticipated, the diopside and hedenbergite contain barely detectable amounts of Fe^{3+} ($\text{Fe}^{3+}/\Sigma\text{Fe}$ of $0.03\pm 0.02(1\sigma)$ and $0.05\pm 0.02(1\sigma)$, respectively). Conversely, the two aegirine crystals are dominated by Fe^{3+} but still contain but appreciable Fe^{2+} ($\text{Fe}^{3+}/\Sigma\text{Fe}$ contents of $0.84\pm 0.03(1\sigma)$ and $0.93\pm 0.03(1\sigma)$ in aegirine 1 and aegirine 2, respectively). Augites 1 and 2 contain intermediate $\text{Fe}^{3+}/\Sigma\text{Fe}$ contents of $0.56\pm 0.03(1\sigma)$ and $0.42\pm 0.03(1\sigma)$, respectively. The other clinopyroxene also has an intermediate $\text{Fe}^{3+}/\Sigma\text{Fe}$ value of $0.50\pm 0.05(1\sigma)$ and could be considered as ferrian diopside (Morimoto et al, 1988).

5 Discussion

5.1 Re-evaluating stoichiometric estimates of iron valence

Clinopyroxene $\text{Fe}^{3+}/\Sigma\text{Fe}$ contents determined by Mössbauer spectroscopy are compared with $\text{Fe}^{3+}/\Sigma\text{Fe}$ contents determined by stoichiometry following Droop (1987) in Figure 5A. Uncertainties in $\text{Fe}^{3+}/\Sigma\text{Fe}$ contents from stoichiometry were determined piece-wise using a Monte Carlo approach whereby oxides derived from EPMA were repeatedly resampled ($n = 100$) to distributions described by 1σ analytical uncertainties from counting statistics. This approach does not account for correlated uncertainties in EPMA results nor does it fully propagate the oxide analytical uncertainty to all the cations, It does however provide reasonable, conservative estimates of uncertainties and informs the robustness of our $\text{Fe}^{3+}/\Sigma\text{Fe}$ determinations obtained when EPMA analyses are accurate within the tolerances described in the Methods. For instance, uncertainties in $\text{Fe}^{3+}/\Sigma\text{Fe}$ decrease with increasing FeO_T (Figure 6A), with

the Fe-poor other clinopyroxene subject to considerably larger uncertainties than all the remaining clinopyroxene crystals considered, including those from OIBs discussed in Part II. This trend results from the plateauing of 1σ uncertainties at ~ 0.35 wt.% Fe_2O_3 in our dual-condition setup optimised for high-precision clinopyroxene analyses (Figure 6B), a value that reflects the combined uncertainties in all elements analysed by EPMA rather than the uncertainty of FeO_T analyses alone, and will vary across different sessions and instruments. Estimating uncertainties using counting statistics from routine EPMA setups that typically measure minor elements for 10 s at 10 nA rather than for 30–60 s at 40 nA such as that described by Neave et al (2019) return considerably larger 1σ uncertainties of ~ 0.85 wt.% Fe_2O_3 .

Linear regression shows that $\text{Fe}^{3+}/\Sigma\text{Fe}$ contents determined by stoichiometry following Droop (1987) correlate positively and strongly with $\text{Fe}^{3+}/\Sigma\text{Fe}$ contents determined by Mössbauer spectroscopy ($r^2 = 0.99$), with the mean 1σ prediction interval of the regression (0.035) being comparable to 1σ analytical uncertainties associated with Mössbauer spectroscopy (0.03–0.05). Uncertainties in the $\text{Fe}^{3+}/\Sigma\text{Fe}$ content of augite crystals estimated using the Monte-Carlo approach described above are of a comparable magnitude to those from the regression against Mössbauer spectroscopy ($\sim 0.05(1\sigma)$). Importantly, these uncertainties increase by a factor of three to values in line with previously reported uncertainties ($\sim 0.16(1\sigma)$) when estimated using counting statistics from routine EPMA setups (cf., McGuire et al, 1989). We therefore believe that clinopyroxene $\text{Fe}^{3+}/\Sigma\text{Fe}$ contents can be determined accurately and precisely using the approach of Droop (1987) when EPMA is carried out with sufficient care.

Stoichiometric determinations following Papike (1974) are less successful for the clinopyroxene crystals studied here ($r^2 = 0.92$ with a mean 1σ prediction interval of ~ 0.2), with estimated $\text{Fe}^{3+}/\Sigma\text{Fe}$ for the augite crystals and other clinopyroxene lying 0.2 below a one-to-one relationship (Figure 5B) despite the diopside, hedenbergite and aegirine crystals falling on the one-to-one line. We therefore suggest that the charge balance relationship proposed by Papike (1974), which only describes one mechanism by which Fe^{3+} can be substituted into clinopyroxene, does not provide a robust description of Fe^{3+} abundance in magmatic augites. Moreover, we suggest that using the approach of Papike (1974) may have led McGuire et al (1989) to prematurely discount the utility of estimating clinopyroxene $\text{Fe}^{3+}/\Sigma\text{Fe}$ by stoichiometry. The lower precision of their analyses (0.5–2% and 10–20% relative quoted for majors and minors, respectively, versus $<1\%$ and $<5\%$ (apart from MnO; $<8\%$), respectively, in our study) may have also contributed to the poor correlation between their results from stoichiometry and Mössbauer spectroscopy, much as it motivated the scepticism of Canil and O'Neill (1996).

5.2 Accounting for ferric iron in clinopyroxene componentry

The componentry scheme described by Putirka et al (1996) is widely used as the basis for empirical thermobarometers (e.g., Putirka, 2008; Neave and Putirka, 2017). This scheme forms Jd first, and also incorporates Ti via a titanium pyroxene component (CaTi ; $\text{CaTiAl}_2\text{O}_6$) through the TiAl_2 – MgSi_2 exchange (Robinson, 1980; Sack and Carmichael, 1984). Despite the subsequent addition of Cr to the scheme via a chromium Tschermak's component (CrCaTs ; $\text{CaCr}_2\text{SiO}_6$) in its later modification by

Putirka et al (2003), this scheme still does not account for the presence of Fe^{3+} . This is at least partly because of the assumed absence of Fe^{3+} from the graphite-buffered experiments reported by Putirka et al (1996). We also speculate that it may reflect an absence of coherent Fe^{3+} systematics estimated from legacy EPMA datasets using stoichiometric criteria, especially when the approach of Papike (1974) was applied.

An alternative scheme described by Sack and Ghiorso (1994a,b) and implemented in the MELTS algorithm (e.g., Ghiorso and Sack, 1995) incorporates Ti via the fictive buffonite (Bf; $\text{CaMg}_{0.5}\text{Ti}_{0.5}\text{Fe}^{3+}\text{SiO}_6$) and alumino-buffonite (ABf; $\text{CaMg}_{0.5}\text{Ti}_{0.5}\text{AlSiO}_6$) components on the basis of miscibility gaps in the Di–CaTi–CaTs ternary and combined TiAl_2 – MgSi_2 , Al– Fe^{3+} and Al_2 – MgSi exchanges observed in natural samples; ABf falls halfway between Di and CaTi, and Bf is related to ABf by Al– Fe^{3+} exchange. Ferric iron is also incorporated within Es via Al– Fe^{3+} exchange with CaTs; Es also hosts Fe^{3+} in the database described by Jennings and Holland (2015) and used in the THERMOCALC algorithm (e.g., Powell et al, 1998). However, recent experiments and Fe-XANES spectroscopy designed to investigate Fe^{3+} partitioning between clinopyroxene and andesitic liquids demonstrate that calculations with the MELTS algorithm systematically and dramatically overestimate clinopyroxene Fe^{3+} contents (Rudra and Hirschmann, 2022), casting doubt on our ability to use thermodynamically constrained but seemingly inaccurate models of Sack and Ghiorso (1994a,b) to assign clinopyroxene components. Reasons for this discrepancy between recent experiments and outputs from the MELTS algorithm may reflect a combination of inaccurate stoichiometric estimates of clinopyroxene Fe^{3+} contents in the calibration database as well as a bias towards experiments on alkaline compositions at low pressures and highly oxidising conditions. A new empirical scheme for assigning clinopyroxene components is therefore needed to provide a complete if empirical description of clinopyroxene compositions in light of our ability to reliably estimate clinopyroxene Fe^{3+} via optimised EPMA.

We propose that components in magmatic clinopyroxene crystals can be calculated using the following scheme based on that described by Putirka et al (1996):

1. Calculate clinopyroxene cation fractions (X_{cation}) from oxide concentrations on a six oxygen basis
2. Determine clinopyroxene $X_{\text{Fe}^{2+}}$ and $X_{\text{Fe}^{3+}}$ contents following Droop (1987) encompassing the renormalisation of cations (including total Fe) by multiplying each cation by T/S as outlined in his point (iv); the total number of all original cations will now equal four and values of $X_{\text{Fe}^{2+}}$ and $X_{\text{Fe}^{3+}}$ can be used to convert FeO_T into FeO and Fe_2O_3
3. Determine the relative proportions of tetrahedral and octahedral Al (Al^{IV} and Al^{VI} , respectively) such that $X_{\text{Al}^{\text{IV}}} = 2 - X_{\text{Si}}$ and $X_{\text{Al}^{\text{VI}}} = X_{\text{Al}} - X_{\text{Al}^{\text{IV}}}$; if X_{Si} exceeds 2 there is no $X_{\text{Al}^{\text{IV}}}$
4. Form Jd ($\text{NaAlSi}_2\text{O}_6$) from whichever is less between Na and Al^{VI} such that $X_{\text{Jd}} = X_{\text{Na}}$ or $X_{\text{Jd}} = X_{\text{Al}^{\text{VI}}}$
5. Form Ae ($\text{NaFe}^{3+}\text{Si}_2\text{O}_6$) from whichever is less between Na remaining after Jd formation and Fe^{3+} such that $X_{\text{Ae}} = X_{\text{Na}} - X_{\text{Jd}}$ or $X_{\text{Ae}} = X_{\text{Fe}^{3+}}$
6. Form neptunite (Np; $\text{NaFe}_{0.5}^{2+}\text{Ti}_{0.5}\text{Si}_2\text{O}_6$) from any Na remaining after Ae formation such that $X_{\text{Np}} = X_{\text{Na}} - X_{\text{Jd}} - X_{\text{Ae}}$; only relevant for alkali clinopyroxenes

7. Form Es ($\text{CaFe}^{3+}\text{AlSiO}_6$) from any Fe^{3+} remaining after Ae formation such that $X_{\text{Es}} = X_{\text{Fe}^{3+}} - X_{\text{Ae}}$
8. Form CaTs (CaAlAlSiO_6) from any $X_{\text{Al}^{\text{VI}}}$ remaining after Jd formation such that $X_{\text{CaTs}} = X_{\text{Al}^{\text{VI}}} - X_{\text{Jd}}$
9. Form CaTi ($\text{CaTiAl}_2\text{O}_6$) from any Ti remaining after Np formation such that $X_{\text{CaTi}} = X_{\text{Ti}} - X_{\text{Np}}/2$; Np is only present in alkali clinopyroxenes
10. Form chromium-aluminium Tschermak's component (CrAlTs; CaCrAlSiO_6) from Cr such that $X_{\text{CrAlTs}} = X_{\text{Cr}}$
11. Form DiHd ($\text{Ca}(\text{Mg}, \text{Fe}^{2+}, \text{Mn})\text{Si}_2\text{O}_6$) from any Ca remaining after Es, CaTs, CaTi and CrAlTs formation such that $X_{\text{DiHd}} = X_{\text{Ca}} - X_{\text{Es}} - X_{\text{CaTs}} - X_{\text{CaTi}} - X_{\text{CrAlTs}}$
12. Form EnFs ($(\text{Mg}, \text{Fe}^{2+}, \text{Mn})_2\text{Si}_2\text{O}_6$) from any Mg, Fe^{2+} and Mn remaining after DiHd formation such that $X_{\text{EnFs}} = (X_{\text{Mg}} + X_{\text{Fe}^{2+}} + X_{\text{Mn}}) - X_{\text{DiHd}}/2$

Although this scheme offers a far from unique solution to describing clinopyroxene compositions, it does account for all relevant elements in an internally consistent way. The results of applying this scheme to our endmember and single-crystal clinopyroxenes is shown in Figure 7 and a worked example in Excel is provided in the Supplementary Material.

Jadeite is formed before Ae in light of experimental and thermodynamic evidence that Na is preferentially incorporated alongside Al^{VI} rather than Fe^{3+} in magmatic clinopyroxenes dominated by quadrilateral components (Sack and Ghiorso, 1994b; Blundy et al, 1995; Putirka et al, 1996; Neave et al, 2019). For example, clinopyroxene Na contents do not correlate with f_{O_2} as would be expected were Na incorporated as Ae. Aegirine is then formed from relatively abundant Fe^{3+} in the case of alkali clinopyroxenes like our aegirine crystals or relatively scarce (or absent) residual Na in the case of all our other clinopyroxene crystals (Figure 7B). Even after Ae component formation, considerable Na remains in the case of aegirine, necessitating the formation of an additional Np component that also accounts for the non-negligible amount of Fe^{2+} present in these crystals (e.g., Ferguson, 1977). Es, the first of several Al^{IV} -bearing components, is formed next from any remaining Fe^{3+} (Figure 7C); Fe^{3+} is usually present in excess over Na in clinopyroxenes dominated by quadrilateral components. Our reasons for favouring Fe^{3+} incorporation into Es are threefold: firstly, Es is considered to be a major reservoir of Fe^{3+} in mantle clinopyroxenes despite their higher Na: Fe^{3+} than many magmatic clinopyroxenes (Luth and Canil, 1993; Blundy et al, 1995; Stolper et al, 2020); secondly, sufficient Al^{IV} is generally present alongside Si in magmatic clinopyroxene crystals to completely fill T sites without needing to incorporate tetrahedral Fe^{3+} (Morimoto et al, 1988), though some tetrahedral Fe^{3+} may occur in clinopyroxene crystals from the mantle (McGuire et al, 1991); and finally, there is tentative evidence that Fe^{3+} correlates with Ca in crystallisation experiments under variable f_{O_2} conditions (Neave et al, 2019).

In line with Putirka et al (1996), CaTs is formed from any Al^{VI} remaining after Jd formation, though we note that CaTs is absent from our endmember clinopyroxene crystals and only occurs in the augite single crystals (Figure 7D). In contrast with Putirka et al (1996), CaTi is then formed from Ti instead of Al^{IV} (Figure 7E). We do this because the approach of Putirka et al (1996) can overestimate the abundance of CaTi by ignoring other Al^{IV} -bearing components (i.e., Es and CrAlTs), and thus

can imply that more Ti is incorporated into clinopyroxene crystals than is actually measured by EPMA. Nonetheless, the behaviour of Ti may be more complicated than captured by our proposed scheme. For example, Ti may be balanced by minor Cr or Fe^{3+} on T sites (Morimoto et al, 1988), potentially via the fictive buffonite component (Bf; $\text{CaMg}_{0.5}\text{Ti}_{0.5}\text{Fe}^{3+}\text{SiO}_6$) of Sack and Ghiorso (1994b). It may also manifest as ABf or a generalised $\text{NaR}_{0.5}^{2+}\text{Ti}_{0.5}\text{Si}_2\text{O}_6$ component.

In contrast with Putirka et al (2003) who incorporate Cr via CrCaTs with Cr on both M1 and T sites, we incorporate Cr in chromium-aluminium Tschermak’s component (CrAlTs; CaCrAlSiO_6). This restriction of Cr to the M1 site agrees with Cr distributions in synthetic clinopyroxenes and conventions about reporting chrome diopside compositions (Robinson, 1980; Akasaka et al, 2019). Both augite crystals and the other clinopyroxene contain variable but meaningful amounts of Cr (Figure 7F).

DiHd is formed from any Ca remaining after the formation of non-quadrilateral components. Our diopside and hedenbergite fall very close to pure DiHd component, as does the other clinopyroxene. As anticipated, our augite crystals are also rich in DiHd, while our aegirine crystals are almost devoid of DiHd (Figure 7G). Finally, EnFs is formed from any Mg, Fe^{2+} and Mn remaining after DiHd formation, and occurs at low but non-negligible levels across all endmember and single-crystal clinopyroxenes (Figure 7H). Note that we group Mn and Fe^{2+} to avoid introducing additional Mn-bearing components. Our new scheme returns component sums within 0.01 of 1, indicating that all elements are suitably accounted for. Furthermore, the sums of Al^{IV} -bearing components formed from other elements (i.e., $X_{\text{Es}} + X_{\text{CaTs}} + X_{\text{CaTi}} + X_{\text{CrAlTs}}$) are within 0.001 of $X_{\text{Al}^{\text{IV}}}$ calculated from $2 - X_{\text{Si}}$.

6 Conclusions

Integrating optimised EPMA analyses of endmember and single-crystal clinopyroxenes with Mössbauer spectroscopy reveals that clinopyroxene $\text{Fe}^{3+}/\Sigma\text{Fe}$ contents can be determined with high accuracy and precision ($1\sigma \sim 3.5\%$ absolute) using established stoichiometric approaches described by Droop (1987). This contrasts with literature opinion (McGuire et al, 1989; Canil and O’Neill, 1996). However, this apparent conflict likely reflects the better performance of the Droop (1987) approach when applied to magmatic clinopyroxene with respect to the popular Papike (1974) approach as well as the optimisation of analytical methods. Nevertheless, further work is required to determine the suitability of using currently available clinopyroxene standards to validate the accuracy of EPMA data used for determining clinopyroxene $\text{Fe}^{3+}/\Sigma\text{Fe}$.

Deriving a scheme for assigning clinopyroxene components that explicitly accounts for Fe^{3+} is a key implication of being able to routinely determine clinopyroxene $\text{Fe}^{3+}/\Sigma\text{Fe}$ contents with a geologically useful level of precision, especially when averaging over large numbers of analyses per crystal. By integrating published observations from natural and experimental systems with our analyses, we propose that most Fe^{3+} is incorporated as Es; substantial amounts of Fe^{3+} are only present in Ae in alkali-rich pyroxenes. By changing how Ti and Cr are assigned to Al^{IV} -bearing components we also improve previous schemes by correctly balancing Al^{IV} and Al^{VI} against the other cations present. We emphasise that the the outputs of our scheme cannot be used

in place of those from prior schemes used for clinopyroxene thermobarometry (e.g., Putirka, 2008). We nonetheless hope that our revised approach to clinopyroxene componentry offers a framework for providing more complete descriptions of clinopyroxene compositions in future as outlined in Part II on clinopyroxene crystals from OIBs.

Acknowledgements

We thank Lee Paul, David Olivier and Lewis Hughes at the University of Manchester for their help with sample preparation, thin section cutting and scanning electron microscopy, respectively. We also thank Stuart Kearns and Ben Buse for their help with electron probe microanalysis at the University of Bristol. Mandy Edwards and David Gelsthorpe facilitated access to collections at the University of Manchester and Manchester Museum, respectively. Olivier Namur provided valuable feedback on an earlier version of the manuscript. This work was supported by a NERC Independent Research Fellowship (NE/T011106/1) and Royal Society Research Grant (RGS\R1\201344).

References

- Akasaka M, Takasu Y, Handa M, et al (2019) Distribution of Cr^{3+} between octahedral and tetrahedral sites in synthetic blue and green $(\text{CaMgSi}_2\text{O}_6)_{95}(\text{CaCrAlSiO}_6)_5$ diopsides. *Mineralogical Magazine* 83(4):497–505. <https://doi.org/10.1180/mgm.2019.1>
- Blundy JD, Falloon TJ, Wood BJ, et al (1995) Sodium partitioning between clinopyroxene and silicate melts. *Journal of Geophysical Research: Solid Earth* 100(B8):15501–15515
- Brounce M, Stolper E, Eiler J (2017) Redox variations in Mauna Kea lavas, the oxygen fugacity of the Hawaiian plume, and the role of volcanic gases in Earth's oxygenation. *Proceedings of the National Academy of Sciences* 114(34):8997–9002. <https://doi.org/10.1073/pnas.1619527114>
- Bryan WB, Thompson G, Ludden JN (1981) Compositional variation in normal MORB from 22°–25°N: Mid-Atlantic Ridge and Kane Fracture Zone. *Journal of Geophysical Research* 86(B12):11815–11836. <https://doi.org/10.1029/JB086iB12p11815>
- Canil D, O'Neill HSC (1996) Distribution of Ferric Iron in some Upper-Mantle Assemblages. *Journal of Petrology* 37(3):609–635. <https://doi.org/10.1093/petrology/37.3.609>
- Deer W, Howie RA, Zussman J (2013) *An introduction to the rock-forming minerals*. Mineralogical Society, London
- Droop GTR (1987) A general equation for Estimating Fe^{3+} concentrations in ferromagnesian silicates and oxides from microprobe analyses, using stoichiometric criteria. *Mineralogical Magazine* 51(361):431–435. <https://doi.org/10.1180/minmag.1987.051.361.10>

- Dyar MD, Gunter ME, Delany JS, et al (2002) Systematics in the structure and XANES spectra of pyroxenes, amphiboles, and micas as derived from oriented single crystals. *Canadian Mineralogist* 40(5):1375–1393. <https://doi.org/10.2113/gscanmin.40.5.1375>
- Ferguson AK (1977) The Natural Occurrence of Aegirine-Neptunite Solid Solution. *Contributions to Mineralogy and Petrology* 253:247–253
- Fournelle J, Scott J (2017) Minerals from the Kakanui Volcanic Breccia: A 2017 Look at Geological Reference Materials for EPMA. *Microscopy and Microanalysis* 23(S1):502–503. <https://doi.org/10.1017/S1431927617003191>
- Frost BR (1991) Introduction to oxygen fugacity and its petrologic importance. *Reviews in Mineralogy and Geochemistry* 25:1–9
- Ghiorso MS, Sack RO (1995) Chemical mass transfer in magmatic processes IV. A revised and internally consistent thermodynamic model for the interpolation and extrapolation of liquid-solid equilibria in magmatic systems at elevated temperatures and pressures. *Contributions to Mineralogy and Petrology* 119(2-3):197–212. <https://doi.org/10.1007/BF00307281>
- Green E, Holland T, Powell R (2007) An order-disorder model for omphacitic pyroxenes in the system jadeite-diopside-hedenbergite-acmite, with applications to eclogitic rocks. *American Mineralogist* 92(7):1181–1189. <https://doi.org/10.2138/am.2007.2401>
- Hammer JE, Jacob S, Welsch B, et al (2016) Clinopyroxene in postshield Haleakala ankaramite 1. Efficacy of thermobarometry. *Contributions to Mineralogy and Petrology* 171:7. <https://doi.org/10.1007/s00410-015-1212-x>
- Höfer HE, Brey GP (2007) The iron oxidation state of garnet by electron microprobe: Its determination with the flank method combined with major-element analysis. *American Mineralogist* 92(5-6):873–885. <https://doi.org/10.2138/am.2007.2390>
- Höfer HE, Brey GP, Schulz-Dobrick B, et al (1994) The determination of the oxidation state of iron by the electron microprobe. *European Journal of Mineralogy* 6(3):407–418. <https://doi.org/10.1127/ejm/6/3/0407>
- Holland TJB, Powell R (1998) An internally consistent thermodynamic data set for phases of petrological interest. *Journal of Metamorphic Geology* 16(3):309–343. <https://doi.org/10.1111/j.1525-1314.1998.00140.x>
- Jakobsson SP, Jónsson J, Shido F (1978) Petrology of the western Reykjanes Peninsula, Iceland. *Journal of Petrology* 19(4):669–705. <https://doi.org/10.1093/petrology/19.4.669>

- Jarosewich E, Gooley R, Husler J (1987) Chromium Augite - A New Microprobe Reference Sample. *Geostandards and Geoanalytical Research* 11(2):197–198. <https://doi.org/10.1111/j.1751-908X.1987.tb00027.x>
- Jennings ES, Holland TJB (2015) A simple thermodynamic model for melting of peridotite in the system NCFMASOCr. *Journal of Petrology* pp 1–24. <https://doi.org/10.1093/petrology/egv020>
- Klügel A, Hansteen TH, Galipp K (2005) Magma storage and underplating beneath Cumbre Vieja volcano, La Palma (Canary Islands). *Earth and Planetary Science Letters* 236(1-2):211–226. <https://doi.org/10.1016/j.epsl.2005.04.006>
- Larsen LM (1976) Clinopyroxenes and Coexisting Mafic Minerals from the Alkaline Ilimaussaq Intrusion, South Greenland. *Journal of Petrology* 17(2):258–290. <https://doi.org/10.1093/petrology/17.2.258>
- Leung IS (1974) Sector-zoned Titanaugites: Morphology, Crystal Chemistry, and Growth. *American Mineralogist* 59:127–138
- Lindsley DH (1983) Pyroxene thermometry. *American Mineralogist* 68(5-6):477–493. <https://doi.org/10.1007/BF00372872>
- Luth RW, Canil D (1993) Ferric iron in mantle-derived pyroxenes and a new oxybarometer for the mantle. *Contributions to Mineralogy and Petrology* 113(2):236–248. <https://doi.org/10.1007/BF00283231>
- MacLennan J, McKenzie D, Grönvold K, et al (2003) Melt mixing and crystallization under Theistareykir, northeast Iceland. *Geochemistry, Geophysics, Geosystems* 4(11):1–40. <https://doi.org/10.1029/2003GC000558>
- McCammon C (2021) Mössbauer Spectroscopy with High Spatial Resolution: Spotlight on Geoscience. In: Yoshida Y, Langouche G (eds) *Modern Mössbauer Spectroscopy*, vol 137. Springer Singapore, Singapore, p 221–266. https://doi.org/10.1007/978-981-15-9422-9_5
- McCammon CA (1994) A Mössbauer milliprobe: Practical considerations. *Hyperfine Interactions* 92:1235–1239. <https://doi.org/10.1007/BF02065761>
- McGuire AV, Dyar MD, Ward KA (1989) Neglected Fe³⁺/Fe²⁺ ratios – a study of Fe³⁺ content of megacrysts from alkali basalts. *Geology* 17(8):687–690. [https://doi.org/10.1130/0091-7613\(1989\)017<0687:NFFRAS>2.3.CO](https://doi.org/10.1130/0091-7613(1989)017<0687:NFFRAS>2.3.CO)
- McGuire AV, Dyar MD, Nielson JE (1991) Metasomatic oxidation of upper mantle peridotite. *Contributions to Mineralogy and Petrology* 109(2):252–264. <https://doi.org/10.1007/BF00306483>, URL <http://link.springer.com/10.1007/BF00306483>

- Mollo S, Del Gaudio P, Ventura G, et al (2010) Dependence of clinopyroxene composition on cooling rate in basaltic magmas: Implications for thermobarometry. *Lithos* 118(3-4):302–312. <https://doi.org/10.1016/j.lithos.2010.05.006>
- Mollo S, Putirka KD, Misiti V, et al (2013) A new test for equilibrium based on clinopyroxene-melt pairs: Clues on the solidification temperatures of Etnean alkaline melts at post-eruptive conditions. *Chemical Geology* 352:92–100. <https://doi.org/10.1016/j.chemgeo.2013.05.026>
- Morimoto N, Fabries J, Ferguson AK, et al (1988) Nomenclature of pyroxenes. *American Mineralogist* 73:1123–1133. <https://doi.org/10.1007/BF01226262>
- Moussallam Y, Edmonds M, Scaillet B, et al (2016) The impact of degassing on the oxidation state of basaltic magmas: A case study of Kīlauea volcano. *Earth and Planetary Science Letters* 450:317–325. <https://doi.org/10.1016/j.epsl.2016.06.031>
- Moussallam Y, Longpré MA, McCammon CA, et al (2019) Mantle plumes are oxidised. *Earth and Planetary Science Letters* 527:115798. <https://doi.org/10.1016/j.epsl.2019.115798>
- Neave DA, Putirka KD (2017) A new clinopyroxene-liquid barometer, and implications for magma storage pressures under Icelandic rift zones. *American Mineralogist* 102:777–794. <https://doi.org/10.2138/am-2017-5968>
- Neave DA, Bali E, Guðfinnsson GH, et al (2019) Clinopyroxene-liquid equilibria and geothermobarometry in natural and experimental tholeiites: the 2014–2015 Holuhraun eruption, Iceland. *Journal of Petrology* 60:1653–1680. <https://doi.org/10.1093/petrology/egz042>
- Papike JJ (1974) Amphiboles and pyroxenes : Characterization of other than quadrilateral components estimates of ferric iron from microprobe data. *Geological Society of America Abstract with Programs* 6:1053–1054
- Petrone CM, Bugatti G, Braschi E, et al (2016) Pre-eruptive magmatic processes re-timed using a non-isothermal approach to magma chamber dynamics. *Nature Communications* 7:12946. <https://doi.org/10.1038/ncomms12946>
- Powell R, Holland TJB, Worley N (1998) Calculating phase diagrams involving solid solutions via non-linear equations, with examples using THERMOCALC. *Journal of Metamorphic Geology* 16:577–588. <https://doi.org/10.1111/j.1525-1314.1998.00157.x>
- Prescher C, McCammon C, Dubrovinsky L (2012) *MossA*: a program for analyzing energy-domain Mössbauer spectra from conventional and synchrotron sources. *Journal of Applied Crystallography* 45(2):329–331. <https://doi.org/10.1107/S0021889812004979>

- Putirka KD (2008) Thermometers and Barometers for Volcanic Systems. *Reviews in Mineralogy and Geochemistry* 69(1):61–120. <https://doi.org/10.2138/rmg.2008.69.3>
- Putirka KD, Johnson M, Kinzler RJ, et al (1996) Thermobarometry of mafic igneous rocks based on clinopyroxene-liquid equilibria, 0–30 kbar. *Contributions to Mineralogy and Petrology* 123(1):92–108. <https://doi.org/10.1007/s004100050145>
- Putirka KD, Mikaelian H, Ryerson F, et al (2003) New clinopyroxene-liquid thermobarometers for mafic, evolved, and volatile-bearing lava compositions, with applications to lavas from Tibet and the Snake River Plain, Idaho. *American Mineralogist* 88(10):1542–1554. <https://doi.org/10.2138/am.2005.431>
- Reay A, Johnstone R, Kawachi Y (1989) Kaersutite, a possible international microprobe standard. *Geostandards and Geoanalytical Research* 13(1):187–190. <https://doi.org/10.1111/j.1751-908X.1989.tb00471.x>
- Robinson P (1980) The composition space of terrestrial pyroxenes -internal and external limits. *Reviews in Mineralogy and Geochemistry* 7:419–494. <https://doi.org/10.1515/9781501508257-013>
- Rudra A, Hirschmann MM (2022) Fe³⁺ partitioning between clinopyroxene and silicate melt at 1-2.5 GPa: implications for Fe³⁺ content of MORB and OIB source mantle. *Geochimica et Cosmochimica Acta* 328:258–279. <https://doi.org/10.1016/j.gca.2022.04.023>
- Rudra A, Cottrell E, Hirschmann MM (2021) Experimental determination of ferric iron partitioning between pyroxene and melt at 100 kPa. *Chemical Geology* 584:120532. <https://doi.org/10.1016/j.chemgeo.2021.120532>
- Sack RO, Carmichael ISE (1984) Fe₂-Mg₂ and TiAl₂-MgSi₂ exchange reactions between clinopyroxenes and silicate melts. *Contributions to Mineralogy and Petrology* 85(2):103–115. <https://doi.org/10.1007/BF00371701>
- Sack RO, Ghiorso MS (1994a) Thermodynamics of multicomponent pyroxenes: I. Formulation of a general model. *Contributions to Mineralogy and Petrology* 116(3):277–286. <https://doi.org/10.1007/BF00306497>
- Sack RO, Ghiorso MS (1994b) Thermodynamics of multicomponent pyroxenes: III. Calibration of Fe²⁺(Mg)₋₁, TiAl₂(MgSi₂)₋₁, TiFe³⁺₂(MgSi₂)₋₁, AlFe³⁺(MgSi)₋₁, NaAl(CaMg)₋₁, Al₂(MgSi)₋₁ and Ca(Mg)₋₁ exchange reactions between pyroxenes and silicate melts. *Contributions to Mineralogy and Petrology* 118(3):271–296. <https://doi.org/10.1007/BF00306648>
- Shorttle O, Moussallam Y, Hartley ME, et al (2015) Fe-XANES analyses of Reykjanes Ridge basalts: Implications for oceanic crust's role in the solid Earth oxygen cycle. *Earth and Planetary Science Letters* 427:272–285. <https://doi.org/10.1016/j.epsl.2015.07.017>

- Smith DGW, O’Nions RK (1971) Investigations of the LII, III X-ray emission spectra of Fe by the electron microprobe Part I: Some aspects of the Fe LII, III spectra from metallic iron and haematite. *Journal of Physics D: Applied Physics* 4(1):147–159. <https://doi.org/10.1088/0022-3727/4/1/320>
- Sobolev VN, Mccammon CA, Taylor LA, et al (1999) Precise Mössbauer milliprobe determination of ferric iron in rock-forming minerals and limitations of electron microprobe analysis. *American Mineralogist* 84:78–85
- Steven CJ, Dyar MD, McCanta M, et al (2022) The absorption indicatrix as an empirical model to describe anisotropy in X-ray absorption spectra of pyroxenes. *American Mineralogist* 107(4):654–663. <https://doi.org/10.2138/am-2021-7950>
- Stolper EM, Shorttle O, Antoshechkina PM, et al (2020) The effects of solid-solid phase equilibria on the oxygen fugacity of the upper mantle. *American Mineralogist* <https://doi.org/10.2138/am-2020-7162>
- Ubide T, Kamber BS (2018) Volcanic crystals as time capsules of eruption history. *Nature Communications* 9(1):326. <https://doi.org/10.1038/s41467-017-02274-w>
- Ubide T, Mollo S, Zhao JX, et al (2019) Sector-zoned clinopyroxene as a recorder of magma history, eruption triggers, and ascent rates. *Geochimica et Cosmochimica Acta* 251:265–283. <https://doi.org/10.1016/j.gca.2019.02.021>
- Wang X, Hou T, Wang M, et al (2021) A new clinopyroxene thermobarometer for mafic to intermediate magmatic systems. *European Journal of Mineralogy* 33(5):621–637. <https://doi.org/10.5194/ejm-33-621-2021>
- Weis FA, Skogby H, Troll VR, et al (2015) Magmatic water contents determined through clinopyroxene: Examples from the Western Canary Islands, Spain. *Geochemistry, Geophysics, Geosystems* 16:2127–2146. <https://doi.org/10.1002/2015GC005800>
- White JC, Ren M, Parker DF (2005) Variation in mineralogy, temperature, and oxygen fugacity in a suite of strongly peralkaline lavas and tuffs, Pantelleria, Italy. *Canadian Mineralogist* 43(4):1331–1347. <https://doi.org/10.2113/gscanmin.43.4.1331>
- Wieser PE, Kent AJR, Till CB, et al (2023) Barometers Behaving Badly I: Assessing the Influence of Analytical and Experimental Uncertainty on Clinopyroxene Thermobarometry Calculations at Crustal Conditions. *Journal of Petrology* 64(2):1–27. <https://doi.org/10.1093/petrology/egac126>
- Wood BJ, Blundy JD (1997) A predictive model for rare earth element partitioning between clinopyroxene and anhydrous silicate melt. *Contributions to Mineralogy and Petrology* 129(2-3):166–181. <https://doi.org/10.1007/s004100050330>

Zhang HL, Cottrell E, Solheid PA, et al (2018) Determination of Fe³⁺/Fe of XANES basaltic glass standards by Mössbauer spectroscopy and its application to the oxidation state of iron in MORB. *Chemical Geology* 479:166–175. <https://doi.org/10.1016/j.chemgeo.2018.01.006>

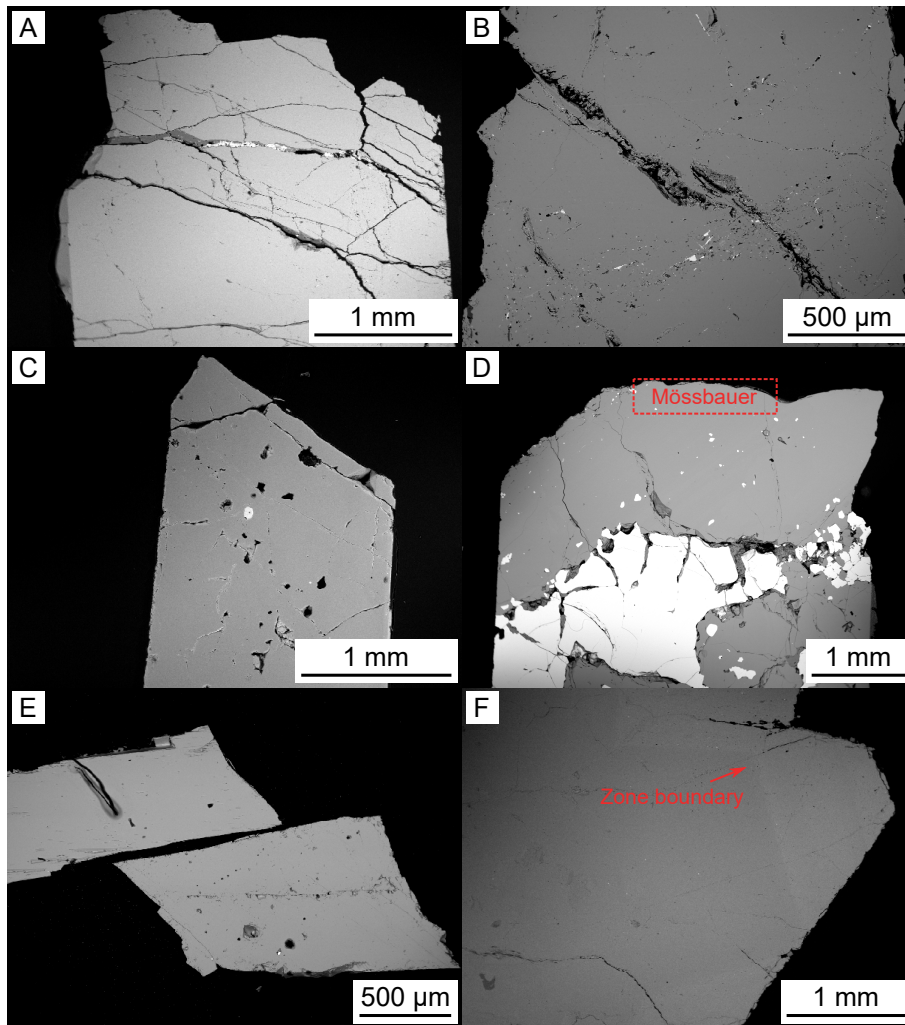


Fig. 1: Backscattered electron (BSE) images of endmember and single-crystal clinopyroxenes. (A) Aegirine 1 shows no evidence for compositional zoning; some fractures contain low volumes of low- and high-BSE-intensity phases. (B) Aegirine 2 shows no evidence for compositional zoning but contains some diffuse bands defined by small crystals of high BSE intensity. (C) Most pieces of augite 1 show no evidence for compositional zoning, but does contain occasional high-BSE-intensity crystals of Fe-Ti oxide as identified from energy dispersive X-ray spectroscopy (EDS). (D) Augite 2 appears compositionally homogeneous but contains abundant high-BSE-intensity inclusions of Fe-Ti oxide. Same material for Mössbauer spectroscopy was mechanically sampled from the inclusion-free portion of the crystal labelled with ‘Mössbauer’. (E) The diopside shows no evidence of compositional zoning. (F) The other clinopyroxene is free of inclusions but shows clear compositional zoning as highlighted with the arrow.

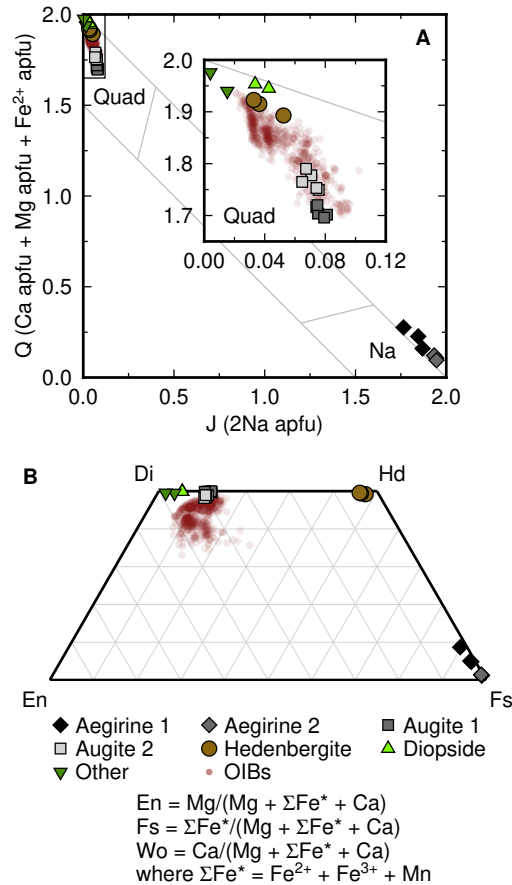


Fig. 2: Classification of endmember and single-crystal clinopyroxenes according to [Morimoto et al \(1988\)](#); clinopyroxenes from ocean island basalts (OIBs) from Iceland and the Azores are shown for comparison (see Part II). (A) Q–J diagram calculated using element abundances as atoms per formula unit (apfu). All clinopyroxene crystals considered are dominated by quadrilateral (Quad) components with the exception of Aegirine 1 and 2. (B) Pyroxene quadrilateral calculated after [Morimoto et al \(1988\)](#) with endmember calculations performed with the Fe component (ΣFe^*) equal to the sum of Fe^{2+} , Fe^{3+} and Mn although Fe^{3+} is not accommodated within quadrilateral components (diopside, Di; hedenbergite, Hd; enstatite, En; and ferrosilite, Fs). Most clinopyroxene compositions fall between Di and Hd; our Diopside and Hedenbergite endmembers are almost pure. Aegirine 1 and 2 fall at the ferrosilite apex, reflecting the absence of Ca-bearing components.

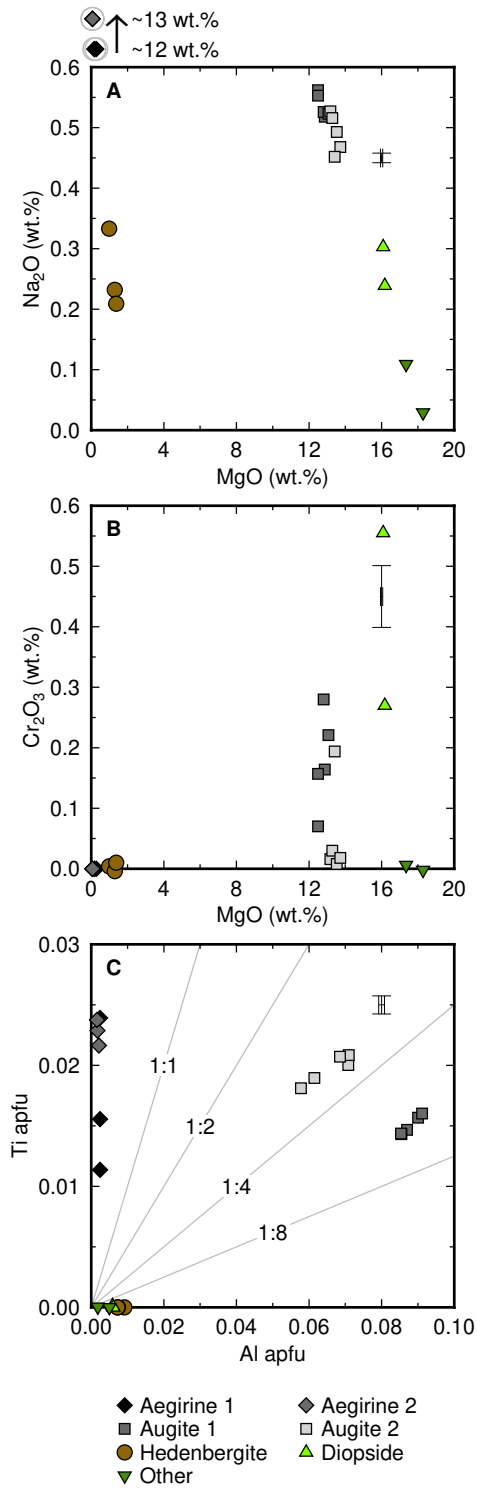


Fig. 3: Summary of key non-quadrilateral major and minor elements in endmember and single crystal clinopyroxenes; 1σ analytical uncertainties are shown. (A) Variation in Na_2O as a function of MgO . (B) Variation in Cr_2O_3 as a function of MgO . (C) Covariation of Ti and Al atoms per formula unit (apfu) calculated on six oxygen basis.

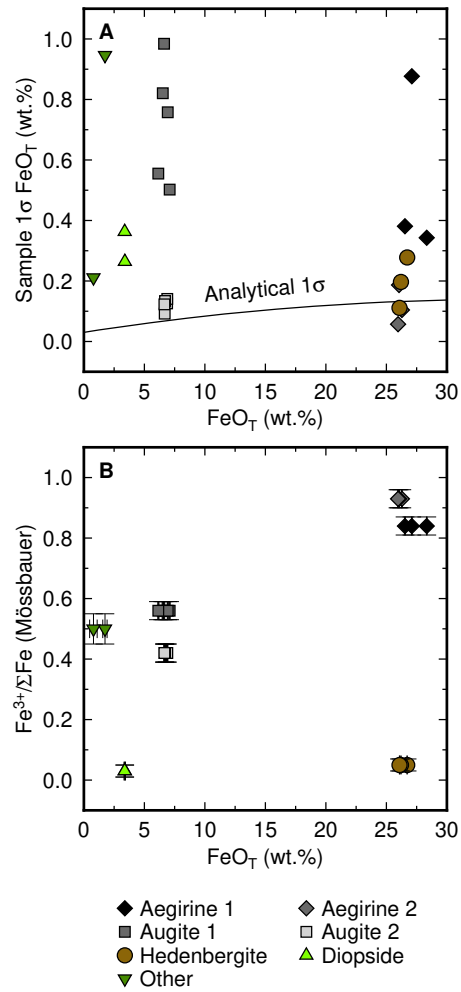


Fig. 4: Iron concentration systematics in endmember and single-crystal clinopyroxenes. (A) Total Fe expressed as FeO (FeO_T) versus the standard deviation of FeO_T in individual pieces of endmember or single-crystal clinopyroxenes. The concentration dependence of 1σ analytical uncertainties from EPMA counting statistics are shown as a black line. Variability in augite 2, aegirine 2 and hedenbergite is comparable with expected analytical uncertainty while variability in other clinopyroxene crystals is out-with the bounds of analytical uncertainty. (B) FeO_T versus the ratio of Fe^{3+} to total Fe ($\text{Fe}^{3+}/\Sigma\text{Fe}$, where $\Sigma\text{Fe} = \text{Fe}^{2+} + \text{Fe}^{3+}$) determined by Mössbauer spectroscopy for powdered aliquots of each clinopyroxene; 1σ analytical uncertainties are shown for Mössbauer data.

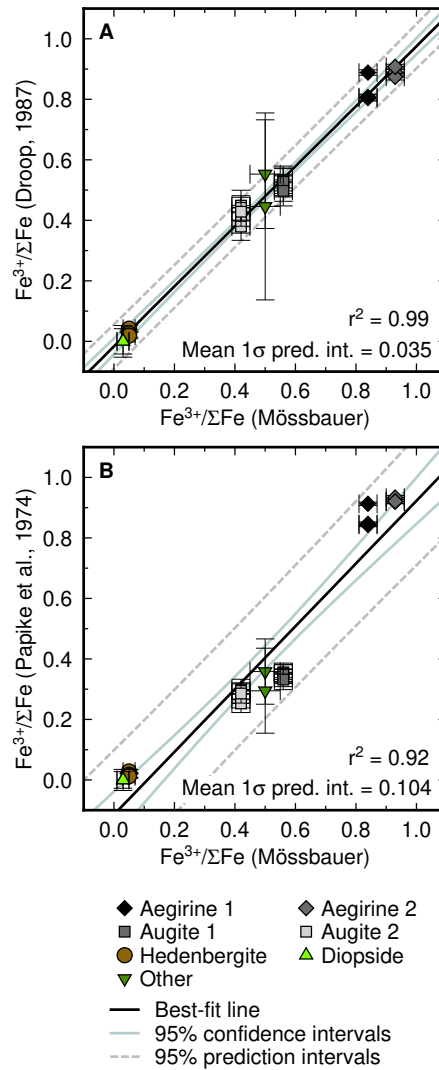


Fig. 5: Iron valence systematics in endmember and single-crystal clinopyroxenes; 1σ uncertainties in stoichiometric determinations were estimated using a Monte-Carlo approach whereby EPMA data were repeatedly resampled according to their analytical uncertainties. (A) $\text{Fe}^{3+}/\Sigma\text{Fe}$ determined by Mössbauer versus $\text{Fe}^{3+}/\Sigma\text{Fe}$ determined by stoichiometry following Droop (1987). Linear regression shows that $\text{Fe}^{3+}/\Sigma\text{Fe}$ calculated following Droop (1987) can reproduce $\text{Fe}^{3+}/\Sigma\text{Fe}$ within the uncertainty of Mössbauer measurements. (B) $\text{Fe}^{3+}/\Sigma\text{Fe}$ determined by Mössbauer versus $\text{Fe}^{3+}/\Sigma\text{Fe}$ determined by stoichiometry following Papike (1974). Although the approach of Papike (1974) can accurately reproduce the $\text{Fe}^{3+}/\Sigma\text{Fe}$ systematics of the diopside, hedenbergite and aegirine crystals, it cannot reproduce the compositions of augite crystals and the other clinopyroxene.

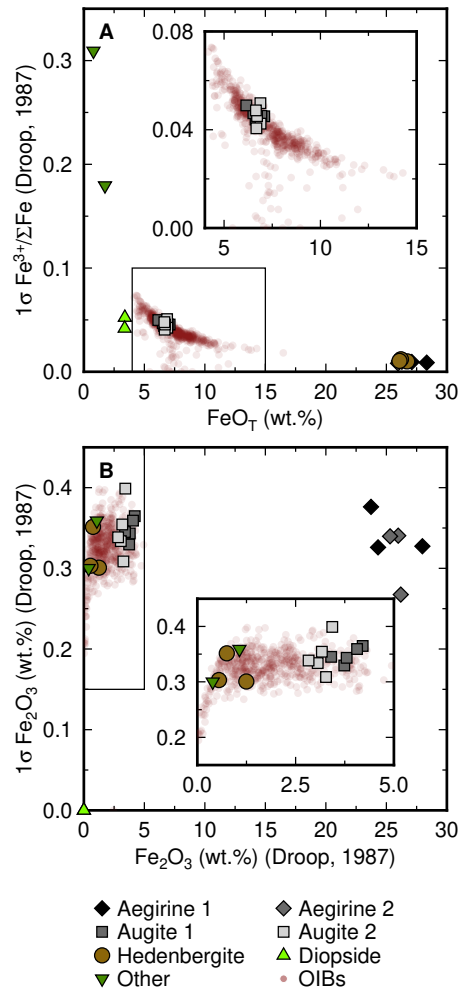


Fig. 6: Estimated uncertainties in clinopyroxene Fe valence and Fe_2O_3 content determined by stoichiometry. Uncertainties in stoichiometric determinations were estimated using a Monte-Carlo approach whereby EPMA data were repeatedly resampled according to their analytical uncertainties. Equivalent uncertainties for clinopyroxenes in OIBs from Iceland and the Azores are shown for comparison (see Part II). (A) $\text{Fe}^{3+}/\Sigma\text{Fe}$ uncertainties in endmember and single-crystal clinopyroxenes determined following Droop (1987) and expressed at the 1σ level as a function of clinopyroxene total Fe expressed as FeO (FeO_T). (B) Fe_2O_3 uncertainties in endmember and single-crystal clinopyroxenes determined following Droop (1987) and expressed at the 1σ level as a function of clinopyroxene Fe_2O_3 content.

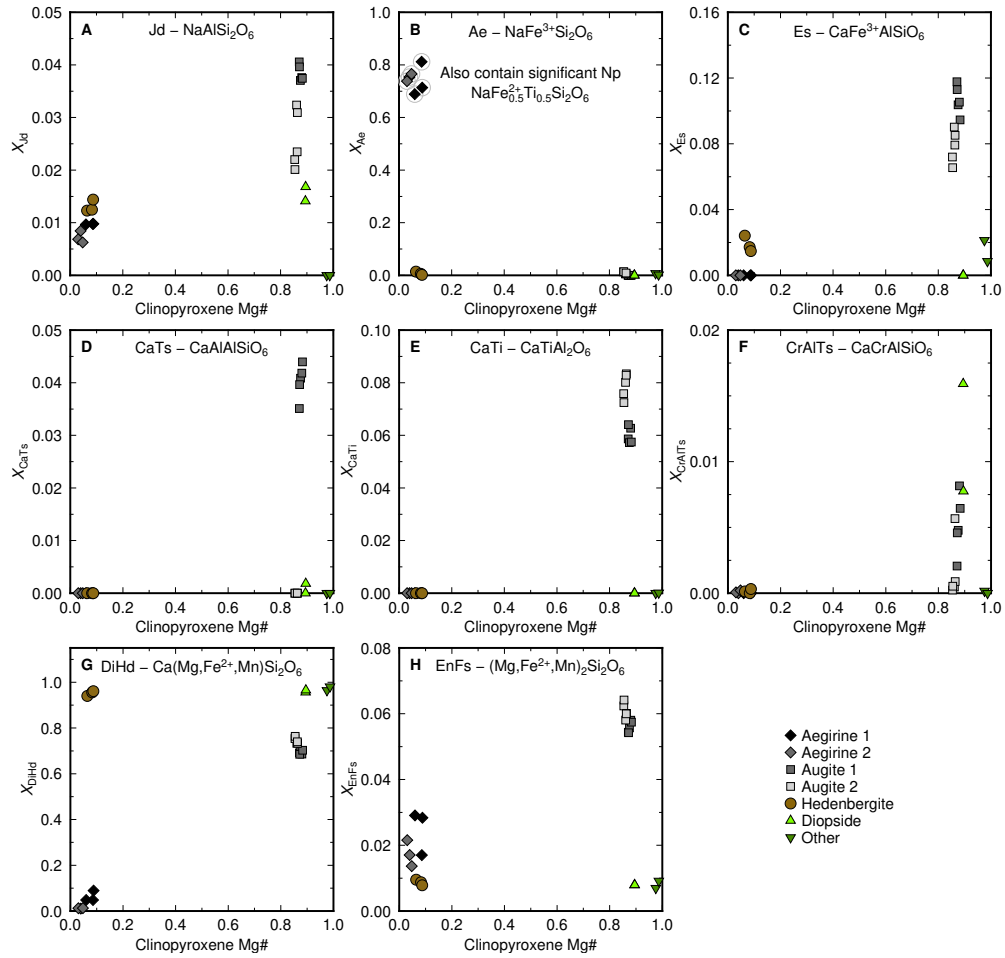


Fig. 7: Clinopyroxene components in endmember and single-crystal clinopyroxenes. Clinopyroxene Mg# is expressed as $\text{Mg}/(\text{Mg}+\text{Fe}^{2+})$ with Fe^{2+} determined following Droop (1987). The scheme for calculating the following components is described in the main text: (A) jadeite, Jd; (B) aegirine, Ae (and neptunite, Np); (C) esseneite, Es; (D) calcium-Tschermak's component, CaTs; (E) titanium pyroxene component, CaTi; (F) chromian calcium-Tschermak's component, CrCaTs; (G) diopside and hedenbergite, DiHd; and (H) enstatite and ferrosilite, EnFs.

Table 1: Endmember and single-crystal clinopyroxene samples studied

Sample	Source	Sample ID	Locality	Sample type
Aegirine 1	DEES ^a	502	Unknown	Single crystals extracted from alkaline igneous rock containing aegirine, feldspar and quartz
Aegirine 2	MM ^b	N3027	Norway	Loose single crystals
Augite 1	DEES	746	Laacher See, Germany	Loose single crystals
Augite 2	DEES	Zn6.6	Unknown	Loose single crystals
Diopside	DEES	4020	Unknown	Large (>1 cm) intergrown crystals of metamorphic diopside
Hedenbergite	DEES	2513	Elba Island, Italy	Small (<1 mm) fibrous intergrown hedenbergite skarn
Other	DEES	499	Unknown	Moderate (~ 5 mm) intergrown, vuggy crystals

^aDepartment of Earth and Environmental Sciences, ^b Manchester Museum

Table 2: Mean compositions of endmember and single-crystal clinopyroxenes determined by EPMA; Fe₂O₃ and FeO contents were determined following [Droop \(1987\)](#)

Sample	Aegirine 1	Aegirine 2	Augite 1	Augite 2	Diopside	Hedenbergite	Other
SiO ₂	52.07	52.03	46.72	47.55	54.90	48.94	55.40
TiO ₂	2.33	3.13	2.16	2.83	0.01	0.00	0.00
Al ₂ O ₃	0.21	0.16	8.06	6.04	0.56	0.66	0.32
Cr ₂ O ₃	0.00	0.00	0.18	0.05	0.41	0.00	0.00
Fe ₂ O ₃	25.34	25.83	3.84	3.15	0.00	0.85	0.73
FeO	4.52	2.86	3.21	3.93	3.38	25.57	0.61
MnO	1.09	1.71	0.11	0.11	0.11	0.89	0.60
MgO	0.21	0.06	12.75	13.42	16.13	1.22	17.81
CaO	1.49	0.29	22.86	22.77	25.05	22.39	25.71
Na ₂ O	12.17	12.93	0.54	0.49	0.27	0.26	0.07
Total	99.43	99.00	100.42	100.35	100.82	100.77	101.26
<i>n</i> EPMA	12	36	32	30	28	12	18
Fe ³⁺ /ΣFe	0.83	0.89	0.52	0.42	0.00	0.03	0.50
Droop (1987)							
Fe ³⁺ /ΣFe	0.84	0.93	0.56	0.42	0.03	0.05	0.50
Mössbauer							